Reconfigurable elastic quantum valley Hall edge states in a piezoelectric topological metamaterial

Dorin, Patrick, Wang, K. W.

Patrick Dorin, K. W. Wang, "Reconfigurable elastic quantum valley Hall edge states in a piezoelectric topological metamaterial," Proc. SPIE 11381, Health Monitoring of Structural and Biological Systems IX, 1138117 (22 April 2020); doi: 10.1117/12.2556854

SPIE.

Event: SPIE Smart Structures + Nondestructive Evaluation, 2020, Online Only, California, United States

Reconfigurable elastic quantum valley Hall edge states in a piezoelectric topological metamaterial

Patrick Dorin*[a], K. W. Wang[a]
[a]Dept. of Mechanical Engineering, University of Michigan, Ann Arbor, MI, USA 48109-2125

ABSTRACT

Unlike conventional elastic waveguides, topologically protected wave transmission in topological metamaterials is immune to backscattering and localization from lattice imperfections and sharp corners. Topologically protected waveguides can be formed by breaking space inversion symmetry within the unit cell of a hexagonal lattice, creating an elastic realization of the quantum valley Hall effect. Recent studies have demonstrated the achievement of tunable topological edge states through the application of an external bias, such as a mechanical, thermal, or magnetic load. These initial studies demonstrate the capability to modify topological edge states through oftentimes complex realizations of truss-like lattice structures or external stimuli. However, a comprehensive reconfigurable topological metamaterial that enables real-time adaptation of both frequency and spatial characteristics of topological properties in an easily integrable manner has yet to be developed. Thus, to advance the state of the art, this research introduces an electromechanical metamaterial with the capability to adjust the frequency range for topological edge states and instantaneously create or eliminate topological interfaces through the integration of piezoelectric circuitry with a continuous mechanical substrate. The metamaterial is comprised of inductor circuitry connected to a thin piezoelectric plate in a periodic manner which produces a hexagonal lattice pattern of electromechanical resonators. The plane wave expansion method is used to reveal a tunable Dirac cone in the band structure of the lattice unit cell and indicate how perturbations to the circuit inductance can open topologically distinct bandgaps. Numerical simulations identify edge modes located at frequencies within the topological bandgap and demonstrate adaptive topologically protected elastic wave transmission.

Keywords: topological, quantum valley Hall, piezoelectric, metamaterial, electromechanical, elastic waveguide, edge states, adaptive

1. INTRODUCTION

Metamaterials are engineered materials that can achieve desirable macroscopic properties and functionalities that are difficult or impossible to achieve with conventional materials. Elastic metamaterials have been studied as a method to control elastic and acoustic waves. Some specific objectives of elastic metamaterial research include, but are not limited to, wave localization, isolation, filtering, sensing, and unidirectional transmission[1–10]. A particular phenomenon that has been investigated is the ability to localize or control elastic wave propagation through the formation of an elastic "waveguide." Confinement of elastic waves within an elastic waveguide enables a variety of applications, such as wave filters, switches, and multiplexers, while also enhancing performance for isolation or energy harvesting systems. In conventional elastic metamaterials, elastic waveguides are generally created by introducing an inclusion into a periodic lattice in the region where you would like to localize the wave[11–16]. While conventional elastic metamaterials are effective at achieving mode localization, performance can be severely degraded by defects or disorder (e.g., sharp corners) in the periodic lattice. In an effort to enhance performance and robustness to defects or disorder that are commonly encountered practical applications, the principles of topological insulators in quantum mechanics[17] have been applied to elastic metamaterial research[18,19]. Topologically protected wave propagation in an elastic waveguide is immune to localization and backscattering in the presence of localized defects and sharp corners, enabling lossless transmission in a myriad of desired directions. This topological protection is achieved by careful engineering of system properties to achieve a topologically non-trivial band structure that is protected by space inversion symmetry (SIS) and time-reversal symmetry (TRS)[20]. The mechanical analogs to topological phenomena found in electronic quantum systems are achievable using either active or passive methods. Previous investigations into the mechanical analog of the electronic quantum Hall effect (QHE), have shown that topologically protected wave transmission can be achieved by breaking TRS with active

*Corresponding Author: Patrick Dorin, email: pdorin@umich.edu

Health Monitoring of Structural and Biological Systems IX, edited by Paul Fromme, Zhongqing Su, Proc. of SPIE Vol. 11381, 1138117 · © 2020 SPIE
CCC code: 0277-786X/20/$21 · doi: 10.1117/12.2556854

spatiotemporal modulation of lattice properties[21–26]. Passive methods have also been investigated to avoid the external power requirements and design challenges associated with the active components (e.g., rotating gyroscopes or electric motors) required to break TRS by the QHE. The mechanical analogs to the quantum spin Hall effect (QSHE) and quantum valley Hall effect (QVHE) both acquire non-trivial topology passively via the breaking of SIS in the lattice while preserving TRS[20]. For the QSHE, two sets of degenerate modes form a double Dirac cone, which, when lifted by a lattice perturbation that breaks SIS, results in two pseudospin modes and topologically protected directional propagation[17,27,28]. While the QSHE does not require active components, the formation of the double Dirac cone can oftentimes require complex mechanisms such as a lattice of pendula[29] or intricate lattice geometries such as sublattices with spatially distinct hexagonal unit cells[30–38]. An alternative to the QSHE with a simpler physical realization is the QVHE. According to the QVHE, a single Dirac cone is formed and protected by TRS, SIS, and C_3 lattice symmetry, and then a bandgap supporting topologically protected edge states is opened by breaking SIS[39–41]. After the demonstration of the acoustic[42] and elastic[43] analogs of the QVHE, there were widespread investigations examining how to leverage the QVHE for topologically protected waveguides. Topologically protected wave transmission from the QVHE was successfully realized by the addition of inclusions or masses to truss-like structures[44] or continuous thin plates[45–52]. While effectively demonstrating the advantages of incorporating topological protection into elastic waveguides, the initial studies included fixed or intricate mechanical systems that operated in a very specific manner once fabricated. Thus, to account for practical manufacturing concerns and variation of external conditions, as well as expand system functionalities, further studies began to explore adaptive topological waveguides. The spatial location of the topological waveguide within a lattice was demonstrated to be reconfigurable via the application of external mechanical[53–58] or magnetic[59] bias. The frequency region for the propagation of edge states was also demonstrated to be tunable with large scale deformation of inflatable embedded structures[60] or thermal loading of temperature-sensitive epoxy[61]. However, a challenge still remains to develop an easily integrable and real-time tunable elastic metamaterial that is capable of adaptation in a wide range of system properties spanning both the frequency and spatial domains. Thus, to advance the state of the art, this research proposes an electromechanical metamaterial with the capability to adjust the frequency, shape, and location of topological edge states. The reconfigurable topological metamaterial is comprised of piezoelectric circuitry that is seamlessly integrated with a thin composite plate, a commonly utilized geometry for a wide range of structural applications requiring load-bearing capability. While the mechanical structure is geometrically homogeneous (thin plate), the circuitry is connected via electrodes that are arranged in a honeycomb lattice formation that contains the symmetries required for the system to exhibit the QVHE. For this study, the piezoelectric circuitry is comprised of an inductor coupled to the piezoelectric capacitor to create a resonant LC circuit. The resonant circuit facilitates the achievement of a Dirac cone at low frequencies corresponding to wavelengths that are larger than the system characteristic wavelength and correspond to the fundamental mode. This ability to achieve subwavelength control of tunable edge states is in contrast to most adaptive topological systems studied to date, which focus only on the short wavelength regime (corresponding to high frequencies), and is an advantage in potential applications that require protected wave control at low frequencies in a compact package.

Integrated piezoelectric circuitry similar to the circuitry contained in the proposed metamaterial has previously been demonstrated as an effective method to achieve active control of bandgap frequencies and wave localization in conventional elastic metamaterials[6,15,62–66]. Recent studies have realized tunable topological wave propagation using piezoelectric circuitry. These studies utilize effective stiffness adaptation of truss-like mechanical lattices to create the QVHE and present specific case studies that demonstrate wave path tunability at high frequencies[67,68]. An additional study investigated adaptive topological wave control via periodic electrical boundary conditions applied to a one-dimensional system (rod)[69]. In contrast, the proposed reconfigurable topological metamaterial achieves a fully comprehensive adaptivity of edge state frequency, shape, and path at low frequencies near the fundamental mode for a two-dimensional system. Protected wave propagation at low frequencies is achieved through resonant circuitry with a tunable inertial term (circuit inductance) that is readily integrated into a continuous load-bearing thin plate that has reduced size requirements due to the subwavelength system characteristic.

In the following manuscript, the governing equations for the proposed reconfigurable metamaterial are derived using the extended Hamilton's principle, and the plane wave expansion method (PWE) is used to identify a tunable Dirac cone in the band structure of the unit cell. Numerical simulations identify edge modes located at frequencies within a topological bandgap generated by perturbation of the circuit inductance parameter and demonstrate elastic wave path tunability. Finally, overall discussion and conclusion are presented.

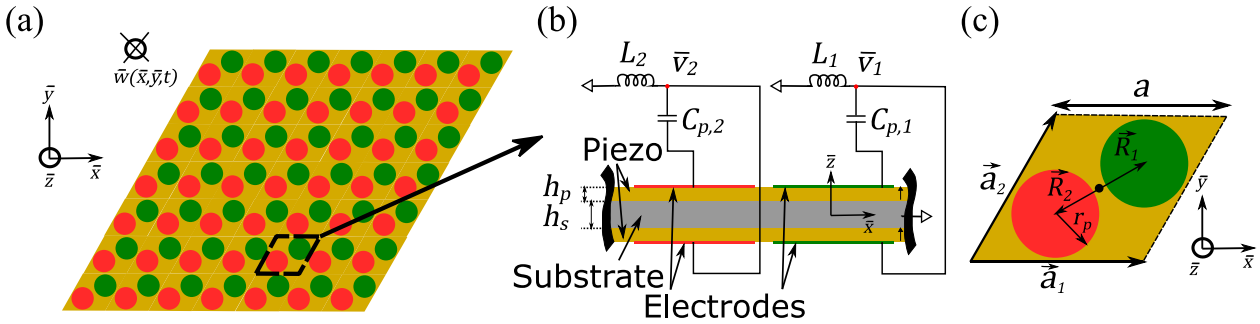

Figure 1. Top view (a) of the proposed piezoelectric metamaterial lattice structure. Cross-section view (b) and top view (c) of the periodic unit cell of the honeycomb lattice. Green indicates electrode geometry related to circuit 1, and red indicates geometry related to circuit 2 of the unit cell. In (a) and (c), the circuity has been omitted for clarity in the description of lattice geometry.

2. SYSTEM DESCRIPTION AND MATHEMATICAL MODEL

2.1 Metamaterial description

The proposed metamaterial (Figure 1) is comprised of an infinite thin composite plate that includes a mechanical substrate (shown in gray) and two piezoelectric layers (yellow). The piezoelectric layers are connected via circular conductive electrodes (red and green) to external circuitry in the series configuration. A diagram of the top view of the metamaterial is shown in Figure 1a, where the honeycomb lattice structure is clearly defined by red and green circles indicating electrode pair 1 and electrode pair 2 of the triangular unit cell, which is enclosed in the dashed lines. The unit cell is further depicted in Figure 1b (cross-section view) and Figure 1c (top view), and includes the aforementioned two pairs of electrodes which enable the formation of two capacitors (capacitor 1 and capacitor 2) with capacitance defined as $C_{p,1}$ and $C_{p,2}$. The output voltages measured across capacitor 1 and capacitor 2 are indicated as $\bar{v}_1$ and $\bar{v}_2$, and the series-connected inductances are defined as L_1 and L_2, respectively. The resulting series LC circuits are resonant with a tuning frequency of $\omega_{t,j} = \frac{1}{\sqrt{L_j C_{p,j}}}$ for the jth circuit. The thicknesses of the substrate and piezoelectric layers are h_s and h_p, respectively, while the thickness of the electrodes is assumed to be negligible in this study. The circular electrodes have a radius r_p and are centered at $\vec{R}_1 = \frac{a}{2\sqrt{3}}\left(\cos\frac{\pi}{6}\hat{\imath} + \sin\frac{\pi}{6}\hat{\jmath}\right)$ for capacitor 1 and $\vec{R}_2 = \frac{-a}{2\sqrt{3}}\left(\cos\frac{\pi}{6}\hat{\imath} + \sin\frac{\pi}{6}\hat{\jmath}\right)$ for capacitor 2 within the unit cell. To form the metamaterial, the unit cell is periodically repeated in the directions of the basis vectors of the direct lattice $\vec{a}_1 = a\hat{\imath}$ and $\vec{a}_2 = a\left(\cos\frac{\pi}{3}\hat{\imath} + \sin\frac{\pi}{3}\hat{\jmath}\right)$. When the circuit parameters of the unit cell (L_1 and L_2) are defined to be identical, the orientation, shape, and location of the electrodes grant the metamaterial C_3 symmetry and SIS. These geometric symmetries, along with TRS, facilitate the mechanical analog of the QVHE. In summary, the proposed topological metamaterial is comprised of a periodic honeycomb lattice with unit cells containing two resonant circuits that are electromechanically coupled to a thin composite plate.

2.2 Governing Equations

A mathematical model governing the system response is derived using the extended Hamilton's Principle,[70] and small deformations are assumed such that classical theory of thin plates[71] and theory of linear piezoelectricity[72] are applicable. The piezoelectric layer and mechanical substrate are assumed to be ideal conductors, and a uniform electric field is assumed for all piezoelectric elements. The governing equations are given by Equation 1 as:

$$D_T \bar{\nabla}^4 \bar{w}(\bar{r},t) + m\frac{\partial^2 \bar{w}(\bar{r},t)}{\partial t^2} - \theta \sum_{j=1}^{N_e} \bar{\nabla}^2 \bar{v}_j(t)\bar{\chi}_j(\bar{r}) = 0 \tag{1a}$$

$$L_j C_{p,j}\frac{\partial^2 \bar{v}_j(t)}{\partial t^2} + \bar{v}_j(t) + \theta \iint_{\bar{D}_j} L_j \frac{\partial^2}{\partial t^2}\bar{\nabla}^2 \bar{w}(\bar{r},t) d^2\bar{r} = 0, \qquad j = 1 \ldots . N_e \text{ electrode pairs} \tag{1b}$$

where $\bar{r} = (\bar{x}, \bar{y})$, $\bar{w}(\bar{r}, t)$ is the flexural displacement of the plate, D_T is the effective flexural rigidity of the composite plate at short circuit, m is the effective mass per unit area of the plate, θ is an electromechanical coupling coefficient, $\bar{v}_j(t)$ is the output voltage across the jth electrode pair, $C_{p,j}$ and L_j are the capacitance and series-connected inductance corresponding to the jth electrode pair, respectively, $\bar{\nabla}^2$ and $\bar{\nabla}^4$, are the Laplacian and biharmonic operator, respectively and N_e is the total number of electrode pairs. In addition, $\bar{\chi}_j$ is a step-function defined as $\bar{\chi}_j(\bar{r}) = \begin{cases} 1, & \bar{r} \in \bar{D}_j \\ 0, & otherwise \end{cases}$, where $\bar{D}_j$ represents the domain containing the jth electrode pair in the $\bar{x} - \bar{y}$ plane. To generalize the results, the governing equations are non-dimensionalized by defining non-dimensional plate displacement, output voltage, time, and spatial length scales (in $\hat{\imath}, \hat{\jmath}, \hat{k}$, directions) as $w = \frac{\bar{w}}{a}, v_j = \frac{1}{a}\frac{C_{p,j}}{\theta}\bar{v}_j, \tau = \sqrt{\frac{1}{L_j C_{p,j}}}t, x = \frac{\bar{x}}{a}$, $y = \frac{\bar{y}}{a}$, and $z = \frac{\bar{z}}{a}$, respectively. A harmonic response at frequency ω is assumed for the plate displacement and electrode output voltage, and non-dimensional variables are substituted as shown in Equation 2:

$$\bar{w}(\bar{r}, t) = aw(r)e^{i\omega\sqrt{L_j C_{p,j}}\tau} \tag{2a}$$

$$\bar{v}_j(t) = \frac{\theta a}{C_{p,j}} v_j e^{i\omega\sqrt{L_j C_{p,j}}\tau} \tag{2b}$$

After substituting results defined in Equation 2 into the governing equations (Equation 1), the resulting non-dimensional governing equations are reduced to the form shown in Equation 3:

$$\left(\nabla^4 - \frac{\omega^2 m a^4}{D_T}\right) w(r) - \sum_{j=1}^{N_e} \frac{\theta^2 a^2}{C_{p,j} D_T} \nabla^2 v_j \chi_j(r) = 0 \tag{3a}$$

$$\left(1 - L_j C_{p,j}\omega^2\right) v_j - \omega^2 L_j C_{p,j} \iint_{D_j} \nabla^2 w(r)\, d^2 r = 0, \qquad j = 1 \ldots . N_e \text{ electrode pairs} \tag{3b}$$

where $r = (x, y)$, and the step-function $\chi_j(r) = \begin{cases} 1, & r \in D_j \\ 0, & otherwise \end{cases}$ is defined in terms of the dimensionless domain D_j of the jth electrode pair.

2.3 Dispersion Relation

Due to the periodicity of the metamaterial, analysis of a single unit cell (Figure 1b, 1c) containing two resonant circuits (N_e= 2) is sufficient to evaluate the dispersion relation. The inductance tuning parameter β is used to specify the inductances for the two circuits in the unit cell as $L_1 = L(1 + \beta)$ and $L_2 = L(1 - \beta)$. When $\beta \neq 0$ the inductance parameters of the two circuits are different, and when the two circuits are defined as identical ($\beta = 0$) the inductance of each circuit is L. To generate the dispersion relation, the non-dimensional plate flexural displacement $w(r)$ is defined as a superposition of plane waves using the PWE method[31,46,73] per Equation 4:

$$\begin{gathered} w(r) = \sum_G W(G) e^{-ia(k+G)\cdot r} \\ G = m\vec{b}_1 + n\vec{b}_2 \quad m, n \in [-M, M] \quad N = 2M + 1 \quad k = \left(k_x, k_y\right) \end{gathered} \tag{4}$$

where G is the reciprocal lattice vector, $\vec{b}_1, \vec{b}_2$ are the basis vectors of the reciprocal lattice, m and n are integers, $W(G)$ is the plane wave coefficient, k is the Bloch wavevector, and M is an integer chosen such that the number of plane waves included for band structure evaluation is $N \times N$. For the triangular unit cell considered here, a schematic of the reciprocal lattice is shown in the inset for Figure 2a, with basis vectors $\vec{b}_1 = \frac{\pi}{a}\left(2\hat{\imath}, -\frac{2}{\sqrt{3}}\hat{\jmath}\right)$ and $\vec{b}_2 = \frac{\pi}{a}\left(0\hat{\imath}, \frac{4}{\sqrt{3}}\hat{\jmath}\right)$. Substituting $w(r)$ from Equation 4 into Equation 3, multiplying by the complex conjugate $e^{ia(k+G)\cdot r}$, and integrating over the unit cell, results in Equation 5:

$$(a^4|k + G|^4 - \Omega^2) W(G) + \vartheta \sum_{j=1}^{N_e} \frac{a^2}{A_c}\frac{a^2}{A_{e,j}} a^2 |k + G|^2 \iint_{D_j} v_j e^{ia(k+G)\cdot r} d^2 r = 0 \tag{5a}$$

$$\left(\frac{\Omega_t^2}{(1-(-1)^j\beta)}-\Omega^2\right)v_j+\Omega^2a^2\sum_G W(G)|k+G|^2\iint_{D_j}e^{-ia(k+G)\cdot r}d^2r=0,\qquad j=1\ldots.N_e \text{ electrode pairs} \qquad (5b)$$

where $\Omega=\omega a^2\sqrt{\frac{m}{D_T}}$ is non-dimensional frequency, $\Omega_t=\omega_t a^2\sqrt{\frac{m}{D_T}}$ is the non-dimensional circuit tuning frequency, $\vartheta=\frac{\theta^2}{\hat{C}_pD_T}$ is a non-dimensional electromechanical coupling coefficient, A_c is the area of the unit cell, and $A_{e,j}$ is the area within the unit cell containing the jth electrode pair. In this model, the surface area of the electrode and the capacitance related to each electrode pair are assumed to be uniform over the unit cell ($A_{e,j}=A_e$, $C_{p,j}=C_p$).

3. DISPERSION ANALYSIS

3.1 Unit Cell

For this study, the composite plate is composed of an aluminum substrate with h_s= 1 mm and PZT-5H piezoelectric layers with h_p= 1 mm, resulting in a dimensionless electromechanical coupling coefficient of ϑ= 0.42. Unit cell characteristic length is defined as a= 0.04 m and electrode size as $A_e=\pi\left(0.92\frac{\sqrt{3}}{6}a\right)^2$ m^2. Equations 5a and 5b can be recast in the form of the classical eigenvalue problem $([\mathbf{K}]-\Omega^2[\mathbf{M}])\begin{bmatrix}\{W_{m,n}\}\\ v_1\\ v_2\end{bmatrix}=0$, and the dispersion relation is solved by specifying the wavevector k along the boundary of the irreducible Brillouin zone (blue triangle in the inset of Figure 2a) and solving for non-dimensional frequency Ω. M= 5 is chosen for computations such that $N\times N$= 121 plane waves are considered. The band structure for the unit cell with identically defined inductance parameters for both circuits ($\beta=0$) and Ω_t= 11 is shown as the solid colored lines in Figure 2a. The finite element tool COMSOL Multiphysics is used to validate the band structure generated by the PWE (open circles in Figure 2a are the COMSOL result). The band structure contains a degeneracy at the K-point in reciprocal space between the first (fundamental) and second modes otherwise referred to as a Dirac point[20] (see dashed box in Figure 2a). The non-dimensional frequency where this Dirac point occurs, or the Dirac frequency, is Ω_{Dirac}= 9. This Dirac point is the vertex of a Dirac Cone that exists in k_x-k_y space, which is protected by C_3 lattice symmetry, SIS, and TRS[20]. While maintaining identical circuit inductance parameters (β= 0), Figure 2b shows how the frequency of the Dirac point (Ω_{Dirac}) varies as a function of the circuit tuning frequency (Ω_t). For a unit cell with specified and homogenous mechanical geometry, the Dirac frequency can be varied between Ω_{Dirac}= 0 and Ω_{Dirac}= 17.5 using only circuit parameters. By specifying the circuit tuning frequency Ω_t, the frequency of the Dirac point can be tuned over a wide frequency region corresponding to the two lowest frequency system modes. Thus, the proposed metamaterial

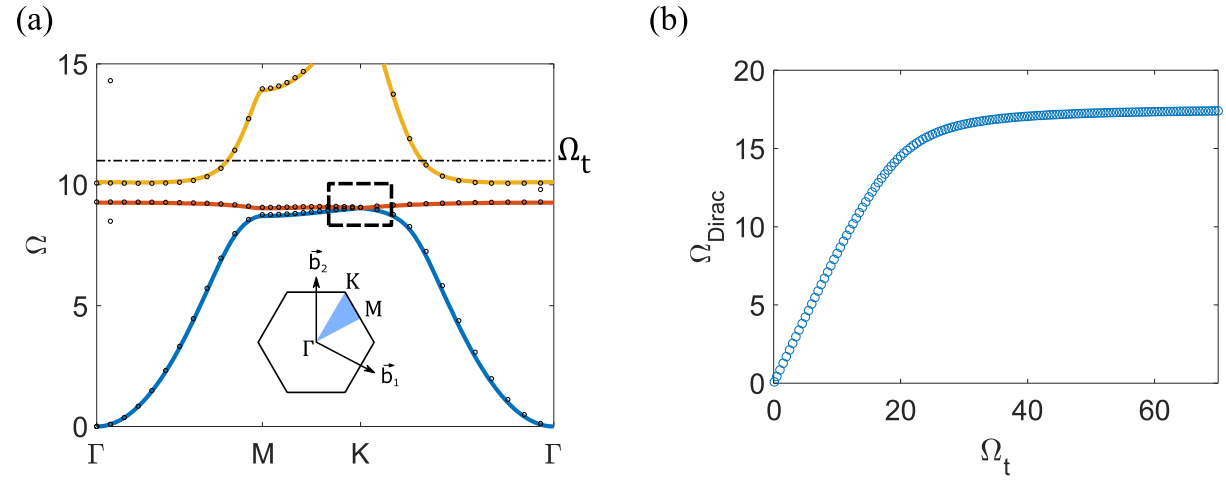

Figure 2. (a) Band structure for the unit cell with $\Omega_t=11$ and $\beta=0$. Bands generated from PWE are marked as solid colored lines, while COMSOL Multiphysics results are marked with open circles. A Dirac point is highlighted by the black dashed box, and a diagram of the reciprocal space is shown in the inset. (b) Dirac frequency Ω_{Dirac} as a function of circuit tuning frequency Ω_t

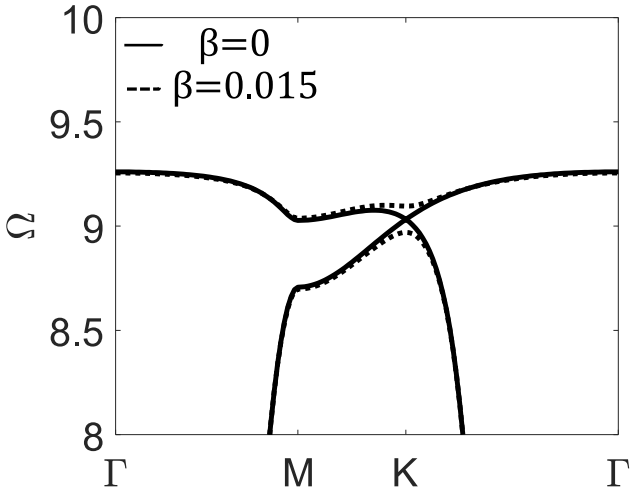

Figure 3. Band diagram containing zoomed-in view of band 1 and band 2 for a unit cell containing SIS β= 0 (solid line) and with broken SIS β= 0.015 (dashed lines) for Ω_t= 11.

is capable of continuously tuning Ω_{Dirac} in a low-frequency region due to the resonant characteristic of the embedded circuits. This continuous frequency tunability of the Dirac point is not a feature of many state of the art adaptive topological waveguides, which generally focus on the realization of path tunability using nonresonant geometric features.

Figure 3 shows a zoomed-in view of the Dirac point for the unit cell with identical circuits (β= 0, solid line Figure 3) and Ω_t= 11. To break the Dirac cone and achieve the elastic analog to the QVHE, SIS must be broken within the unit cell[20,39,74,75]. To break SIS, the two circuits of the unit cell are defined with different inductance parameters ($\beta \neq 0$). A lattice with $\beta > 0$ is defined as Type A, while a lattice with $\beta < 0$ is defined as Type B. For this study, the magnitude of the circuit inductance perturbation in the Type A and Type B lattice types is $|\beta|$ = 0.015. The band structure for a Type A lattice with Ω_t= 11 is shown in Figure 3 (β= 0.015, dashed line Figure 3). By breaking SIS, the degeneracy is lifted, and a full bandgap is created between the first two bands (Ω= 8.90 to Ω= 9.05) (Figure 3)[39,75]. An equal and opposite set of inductance parameters contained by a Type B lattice (β= -0.015) yield an identical band structure (and bandgap frequency range) to that of the Type A lattice (β= 0.015). However, a band inversion exists between the Type A and Type B lattices, as the eigenvectors ($u(k)$) associated with band 1 and band 2 for each lattice are interchanged. The topological properties of these eigenvectors are characterized by the valley Chern number C_{v-p}, which is a topological invariant defined as the integral of the Berry Curvature $B_p(k) = -\nabla_k \times \langle u_p(k)|i\nabla_k[\mathbf{M}]|u_p(k)\rangle$ associated with the pth band near the K-point in reciprocal space ($C_{v-p} = \frac{1}{2\pi}\iint_v B_p(k)d^2k$)[39,55,74,76]. The theoretical valley Chern numbers in a Type A lattice are -0.5 and 0.5 for $C_{v-1}^{Type\ A}$ and $C_{v-2}^{Type\ A}$, respectively. For a Type B lattice these values are equal and opposite ($C_{v-1}^{Type\ B}$= 0.5 and $C_{v-2}^{Type\ B}$ = -0.5). The dissimilar C_{v-p} values indicate that Type A and Type B lattices are topologically distinct. When these two topologically distinct lattices are joined at an interface, a topological transition occurs, and the number of topologically protected interface states (edge states located at the interface between lattice types) located within the bandgap is predicted as $N_{interface-states} = \left|C_{v-k}^{Type\ A} - C_{v-k}^{Type\ B}\right| = 1$[55,74]. For the circuit perturbation chosen in this study ($|\beta|$ = 0.015), the calculated valley Chern numbers are $C_{v-1}^{Type\ A}$= -0.3 and $C_{v-2}^{Type\ A}$ = 0.3 for the Type A lattice and $C_{v-1}^{Type\ B}$= 0.3 and $C_{v-2}^{Type\ B}$ = -0.3 for the Type B lattice. The magnitude of the calculated valley Chern number is less than the theoretically predicted valley Chern number (($|C_{v-calculated}|$= 0.3 < $|C_{v-theoretical}|$= 0.5) due to the relatively large symmetry-breaking perturbation contained in the lattice[45,60]. However, the non-trivial value of the calculated C_{v-p} indicates non-trivial topological characteristics and predicts the emergence of a topologically protected edge state at an interface of adjoined Type A and Type B lattices.

3.2 Finite Strip

A dispersion analysis is conducted for a finite width strip to demonstrate the existence of a topologically protected interface state. The finite strip is comprised of 18 unit cells (Figure 4a). A periodic boundary condition is applied in the $k_{//}$ direction and fixed boundary conditions are applied to the edges. An interface is created at the domain wall between nine Type B unit cells and nine Type A unit cells (dashed box in Figure 4a, circuit parameters defined as $L_I < L_{II}$). The topologically distinct characteristics of Type A and Type B unit cell types (discussed in Section 3.1) create a topological transition at the interface. COMSOL Multiphysics is used to generate the band structure for the finite strip with circuit inductance perturbation defined as $|\beta| = 0.015$ (Figure 4b). A metric is created to evaluate the localization of flexural displacement w

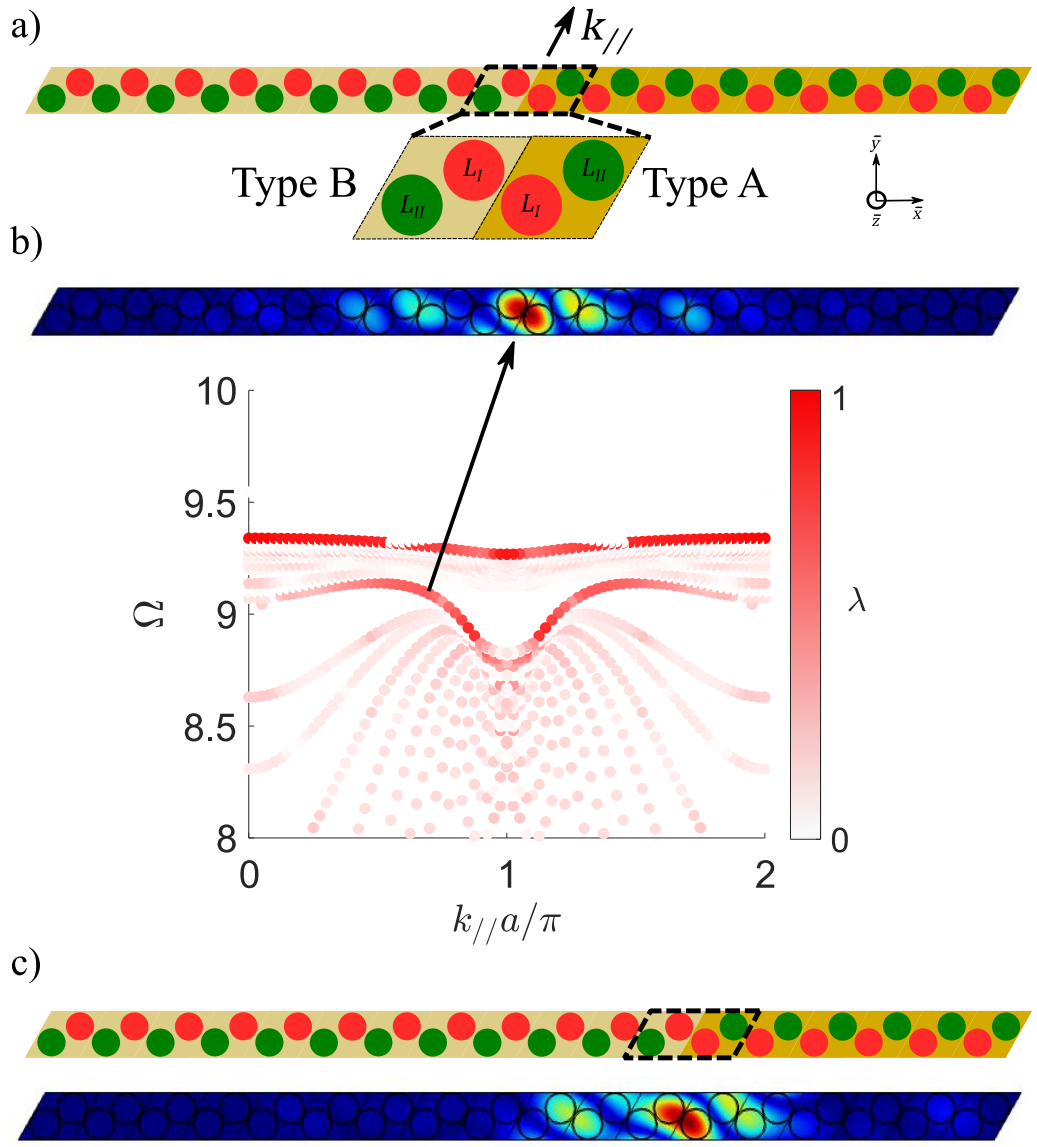

Figure 4. (a) Schematic of finite strip with Type B sublattice indicated as light brown (left) and Type A sublattice indicated as dark yellow (right). Interface is marked by dashed box. Red circles represent electrode pairs connected to L_I, and green circles represent electrode pairs connected to L_{II}. (b) Band structure for finite strip with $|\beta| = 0.015$. Colormap indicates flexural mode displacement localization at interface through localization parameter λ. Dark shaded bands are interface states ($\lambda \cong 1$). Top inset is displacement field of interface mode for $k_{//} = 0.7\pi/a$ and $\Omega = 9.05$. (c) Schematic and interface mode shape for a different interface location.

at the interface, defined as $\lambda = \frac{\iiint_{V_{interface}} |w|^2 dV}{\iiint_{V_S} |w|^2 dV}$, where $V_{interface}$ is the volume of the two adjacent unit cells at the interface (dashed box in Figure 4a) and V_S is the volume of the entire finite strip (Figure 4a). The band structure consists of a color map, with lighter shaded bands representing bulk modes ($\lambda \ll 1$) and darker shaded bands indicating $\lambda \cong 1$ and strong localization of flexural displacement at the interface (i.e., interface states). An interface state (Figure 4b) is observed within the full bandgap that is opened from the Dirac point for the unit cell ($\Omega_{\text{bandgap}} \in [8.90, 9.05]$ for $\Omega_{\text{Dirac}} = 9$), as seen in Section 3.1 (Figure 3). As shown in Section 3.1, the frequency of the Dirac point Ω_{Dirac} can be tailored using embedded circuit parameters. Thus, the frequency range of the associated bandgap and the interface state contained within it is tunable as well. The mode shape for the interface state at $k_{//} = 0.7\pi/a$ and $\Omega = 9.05$ is presented in Figure 4b, clearly showing localization of flexural displacement at the interface. Due to the topological transition present at the interface, this localized interface state is topologically protected (see section 3.1 for explanation). A second localized interface state exists at higher frequencies ($\Omega \cong 9.4$) but is difficult to activate in practice because it is not in the bandgap and easily hybridizes with bulk modes.

In addition to being frequency tunable, the location of the interface state can also be changed using circuit parameters. A schematic of a finite strip with 12 Type B unit cells and six Type A unit cells is shown in Figure 4c. The band structure for this configuration (not shown) is nearly indistinguishable from the band structure shown in Figure 4b. The flexural displacement of the interface mode remains localized at the interface, which has now been moved three cells to the right (Figure 4c) when compared to the original position (Figure 4a). Therefore, the proposed piezoelectric metamaterial enables reconfiguration of both the location and frequency characteristics of the interface state, which could be used to achieve topologically protected wave transmission.

4. CONCLUSIONS

In this study, an adjustable piezoelectric topological metamaterial is proposed and investigated. The metamaterial consists of a thin composite plate that is electromechanically coupled to piezoelectric resonant circuitry through conductive electrodes. While the mechanical structure is geometrically homogeneous and load-bearing, the conductive electrodes are placed in a honeycomb lattice arrangement, which enables the realization of the quantum valley Hall effect. A subwavelength Dirac point is identified in the band structure of the unit cell using the plane wave expansion method. Further investigation of the unit cell band structure indicates that circuit frequency parameters can be used to tune the frequency of the Dirac point and break the degeneracy to open a bandgap. Topologically distinct lattice arrangements are identified by evaluation of the topological invariant (valley Chern number) and combined into a finite width strip with an interface containing a topological transition. A dispersion analysis for the finite width strip reveals a topologically protected interface state with highly localized displacement that is both path and frequency tunable. The end result is a topologically protected waveguide that can be reconfigured in both the spatial and frequency domains to expand functionalities and adjust to changing external conditions. The resonant nature of the circuitry embedded into the metamaterial facilitates subwavelength topological wave transmission and real-time reconfiguration through circuit frequency parameters. Thus, the proposed approach can be used for wave control in low-frequency applications with size constraints and is easily integrated into commonly used load-bearing structures (e.g., thin plate). The comprehensive reconfigurability of the metamaterial could be leveraged to improve robustness and performance for applications such as filtering, multiplexing, isolation, and energy harvesting while encouraging further expansion of topological metamaterial functionalities.

ACKNOWLEDGMENTS

This research is funded by the National Science Foundation under Award No. 1661568. P.D. also acknowledges financial support from the Rackham Merit Fellowship at the University of Michigan.

REFERENCES

[1] Hussein, M. I., Leamy, M. J. and Ruzzene, M., "Dynamics of phononic materials and structures: historical origins, recent progress, and future outlook," Appl. Mech. Rev. 66(4), 040802 (2014).

[2] Zheng, Y., Wu, Z., Zhang, X. and Wang, K. W., "A piezo-metastructure with bistable circuit shunts for adaptive nonreciprocal wave transmission," Smart Mater. Struct. 28(4), 045005 (2019).

[3] Wu, Z. and Wang, K. W., "On the wave propagation analysis and supratransmission prediction of a metastable modular metastructure for adaptive non-reciprocal energy transmission," J. Sound Vib. 458, 389–406 (2019).

[4] Liu, Z., Zhang, X., Mao, Y., Zhu, Y. Y., Yang, Z., Chan, C. T. and Sheng, P., "Locally resonant sonic materials," Science 289(5485), 1734–1736 (2000).

[5] Ma, G. and Sheng, P., "Acoustic metamaterials: From local resonances to broad horizons," Sci. Adv. 2(2), e1501595 (2016).

[6] Thorp, O., Ruzzene, M. and Baz, A., "Attenuation and localization of wave propagation in rods with periodic shunted piezoelectric patches," Smart Mater. Struct. 10(5), 979–989 (2001).

[7] Ho, K. M., Cheng, C. K., Yang, Z., Zhang, X. X. and Sheng, P., "Broadband locally resonant sonic shields," Appl. Phys. Lett. 83(26), 5566–5568 (2003).

[8] Thota, M., Li, S. and Wang, K. W., "Lattice reconfiguration and phononic band-gap adaptation via origami folding," Phys. Rev. B 95(6), 064307 (2017).

[9] Cummer, S. A., Christensen, J. and Alù, A., "Controlling sound with acoustic metamaterials," Nat. Rev. Mater. 1, 16001 (2016).

[10] Liu, X., Cai, G. and Wang, K. W., "Synthesizing and reconfiguring metastable modular metamaterials for adaptive wave propagation control," J. Sound Vib. 468, 115114 (2020).

[11] Oudich, M., Assouar, M. B. and Hou, Z., "Propagation of acoustic waves and waveguiding in a two-dimensional locally resonant phononic crystal plate," Appl. Phys. Lett. 97(19), 193503 (2010).

[12] Thota, M. and Wang, K. W., "Tunable waveguiding in origami phononic structures," J. Sound Vib. 430, 93–100 (2018).

[13] Vasseur, J. O., Deymier, P. A., Djafari-Rouhani, B., Pennec, Y. and Hladky-Hennion, A. C., "Absolute forbidden bands and waveguiding in two-dimensional phononic crystal plates," Phys. Rev. B 77(8), 085415 (2008).

[14] Khelif, A., Djafari-Rouhani, B., Vasseur, J. O. and Deymier, P. A., "Transmission and dispersion relations of perfect and defect-containing waveguide structures in phononic band gap materials," Phys. Rev. B 68(2), 024302 (2003).

[15] Casadei, F., Delpero, T., Bergamini, A., Ermanni, P. and Ruzzene, M., "Piezoelectric resonator arrays for tunable acoustic waveguides and metamaterials," J. Appl. Phys. 112(6), 064902 (2012).

[16] Benchabane, S., Khelif, A., Choujaa, A., Djafari-Rouhani, B. and Laude, V., "Interaction of waveguide and localized modes in a phononic crystal," Europhys. Lett. 71(4), 570–575 (2005).

[17] Hasan, M. Z. and Kane, C. L., "Colloquium: topological insulators," Rev. Mod. Phys. 82(4), 3045–3067 (2010).

[18] Huber, S. D., "Topological mechanics," Nat. Phys. 12(7), 621–623 (2016).

[19] Chen, H., Nassar, H. and Huang, G. L., "A study of topological effects in 1D and 2D mechanical lattices," J. Mech. Phys. Solids 117, 22–36 (2018).

[20] Ma, G., Xiao, M. and Chan, C. T., "Topological phases in acoustic and mechanical systems," Nat. Rev. Phys. 1(4), 281–294 (2019).

[21] Wang, P., Lu, L. and Bertoldi, K., "Topological phononic crystals with one-way elastic edge waves," Phys. Rev. Lett. 115(10), 104302 (2015).

[22] Nash, L. M., Kleckner, D., Read, A., Vitelli, V., Turner, A. M. and Irvine, W. T. M., "Topological mechanics of gyroscopic metamaterials," Proc. Natl. Acad. Sci. 112(47), 14495–14500 (2015).

[23] Wang, Y. T., Luan, P. G. and Zhang, S., "Coriolis force induced topological order for classical mechanical vibrations," New J. Phys. 17(7), 073031 (2015).

[24] Swinteck, N., Matsuo, S., Runge, K., Vasseur, J. O., Lucas, P. and Deymier, P. A., "Bulk elastic waves with unidirectional backscattering-immune topological states in a time-dependent superlattice," J. Appl. Phys. 118(6), 063103 (2015).

[25] von Klitzing, K., "The quantized Hall effect," Rev. Mod. Phys. 58(3), 519 (1986).

[26] Chaunsali, R., Kim, E., Thakkar, A., Kevrekidis, P. G. and Yang, J., "Demonstrating an in situ topological band transition in cylindrical granular chains," Phys. Rev. Lett. 119(2), 024301 (2017).

[27] Kane, C. L. and Mele, E. J., "Quantum spin Hall effect in graphene," Phys. Rev. Lett. 95(22), 226801 (2005).

[28] Wu, L. H. and Hu, X., "Scheme for achieving a topological photonic crystal by using dielectric material," Phys. Rev. Lett. 114(22), 223901 (2015).
[29] Susstrunk, R. and Huber, S. D., "Observation of phononic helical edge states in a mechanical topological insulator," Science 349(6243), 47–50 (2015).
[30] Yves, S., Fleury, R., Lemoult, F., Fink, M. and Lerosey, G., "Topological acoustic polaritons: robust sound manipulation at the subwavelength scale," New J. Phys. 19(7), 075003 (2017).
[31] Chaunsali, R., Chen, C. W. and Yang, J., "Subwavelength and directional control of flexural waves in zone-folding induced topological plates," Phys. Rev. B 97(5), 054307 (2018).
[32] Miniaci, M., Pal, R. K., Morvan, B. and Ruzzene, M., "Experimental observation of topologically protected helical edge modes in patterned elastic plates," Phys. Rev. X 8(3), 031074 (2018).
[33] Yang, L., Yu, K., Wu, Y., Zhao, R. and Liu, S., "Topological spin-Hall edge states of flexural wave in perforated metamaterial plates," J. Phys. D. Appl. Phys. 51(32), 325302 (2018).
[34] Mousavi, S. H., Khanikaev, A. B. and Wang, Z., "Topologically protected elastic waves in phononic metamaterials," Nat. Commun. 6, 8682 (2015).
[35] Li, J., Wang, J., Wu, S. and Mei, J., "Pseudospins and topological edge states in elastic shear waves," AIP Adv. 7(12), 125030 (2017).
[36] He, C., Ni, X., Ge, H., Sun, X. C., Chen, Y. B., Lu, M. H., Liu, X. P. and Chen, Y. F., "Acoustic topological insulator and robust one-way sound transport," Nat. Phys. 12(12), 1124–1129 (2016).
[37] Chaunsali, R., Chen, C. W. and Yang, J., "Experimental demonstration of topological waveguiding in elastic plates with local resonators," New J. Phys. 20(11), 113036 (2018).
[38] Zheng, L. Y., Theocharis, G., Tournat, V. and Gusev, V., "Quasitopological rotational waves in mechanical granular graphene," Phys. Rev. B 97(6), 060101 (2018).
[39] Xiao, D., Yao, W. and Niu, Q., "Valley-contrasting physics in graphene: magnetic moment and topological transport," Phys. Rev. Lett. 99(23), 236809 (2007).
[40] Rycerz, A., Tworzydło, J. and Beenakker, C. W. J., "Valley filter and valley valve in graphene," Nat. Phys. 3(3), 172–175 (2007).
[41] Nakada, K., Fujita, M., Dresselhaus, G. and Dresselhaus, M. S., "Edge state in graphene ribbons: Nanometer size effect and edge shape dependence," Phys. Rev. B 54(24), 17954 (1996).
[42] Zhong, W. and Zhang, X., "Acoustic analog of monolayer graphene and edge states," Phys. Lett. A 375(40), 3533–3536 (2011).
[43] Torrent, D., Mayou, D. and Sánchez-Dehesa, J., "Elastic analog of graphene: Dirac cones and edge states for flexural waves in thin plates," Phys. Rev. B 87(11), 115143 (2013).
[44] Vila, J., Pal, R. K. and Ruzzene, M., "Observation of topological valley modes in an elastic hexagonal lattice," Phys. Rev. B 96(13), 134307 (2017).
[45] Zhu, H., Liu, T. W. and Semperlotti, F., "Design and experimental observation of valley-Hall edge states in diatomic-graphene-like elastic waveguides," Phys. Rev. B 97(17), 174301 (2018).
[46] Pal, R. K. and Ruzzene, M., "Edge waves in plates with resonators: an elastic analogue of the quantum valley Hall effect," New J. Phys. 19(2), 025001 (2017).
[47] Lera, N., Torrent, D., San-Jose, P., Christensen, J. and Alvarez, J. V., "Valley Hall phases in kagome lattices," Phys. Rev. B 99(13), 134102 (2019).
[48] Chen, J. J., Huo, S. Y., Geng, Z. G., Huang, H. B. and Zhu, X. F., "Topological valley transport of plate-mode waves in a homogenous thin plate with periodic stubbed surface," AIP Adv. 7(11), 115215 (2017).
[49] Jin, Y., Torrent, D. and Djafari-Rouhani, B., "Robustness of conventional and topologically protected edge states in phononic crystal plates," Phys. Rev. B 98(5), 054307 (2018).
[50] Ganti, S. S., Liu, T. W. and Semperlotti, F., "Topological edge states in phononic plates with embedded acoustic black holes," J. Sound Vib. 466, 115060 (2020).
[51] Yan, M., Lu, J., Li, F., Deng, W., Huang, X., Ma, J. and Liu, Z., "On-chip valley topological materials for elastic wave manipulation," Nat. Mater. 17(11), 993–998 (2018).
[52] Du, Z., Chen, H. and Huang, G., "Optimal quantum valley Hall insulators by rationally engineering Berry curvature and band structure," J. Mech. Phys. Solids 135, 103784 (2020).
[53] Darabi, A. and Leamy, M. J., "Reconfigurable topological insulator for elastic waves," J. Acoust. Soc. Am. 146(1), 773–781 (2019).
[54] Wu, Y., Chaunsali, R., Yasuda, H., Yu, K. and Yang, J., "Dial-in topological metamaterials based on bistable stewart platform," Sci. Rep. 8, 112 (2018).

[55] Liu, T. W. and Semperlotti, F., "Tunable acoustic valley–Hall edge states in reconfigurable phononic elastic waveguides," Phys. Rev. Appl. 9(1), 014001 (2018).
[56] Tang, K., Makwana, M. P., Craster, R. V. and Sebbah, P., "Observations of symmetry induced topological mode steering in a reconfigurable elastic plate," arXiv Prepr. arXiv1910.08172 (2019).
[57] Li, S., Zhao, D., Niu, H., Zhu, X. and Zang, J., "Observation of elastic topological states in soft materials," Nat. Commun. 9, 1370 (2018).
[58] Süsstrunk, R., Zimmermann, P. and Huber, S. D., "Switchable topological phonon channels," New J. Phys. 19(1), 015013 (2017).
[59] Zhang, Q., Chen, Y., Zhang, K. and Hu, G., "Programmable elastic valley Hall insulator with tunable interface propagation routes," Extrem. Mech. Lett. 28, 76–80 (2019).
[60] Nguyen, B. H., Zhuang, X., Park, H. S. and Rabczuk, T., "Tunable topological bandgaps and frequencies in a pre-stressed soft phononic crystal," J. Appl. Phys. 125(9), 095106 (2019).
[61] Liu, H., Huo, S. Y., Feng, L. Y., Huang, H. B. and Chen, J. J., "Thermally tunable topological edge states for in-plane bulk waves in solid phononic crystals," Ultrasonics 94, 227–234 (2019).
[62] Wang, K. W. and Tang, J., [Adaptive Structural Systems with Piezoelectric Transducer Circuitry], Springer (2008).
[63] Casadei, F., Ruzzene, M., Dozio, L. and Cunefare, K. A., "Broadband vibration control through periodic arrays of resonant shunts: experimental investigation on plates," Smart Mater. Struct. 19(1), 015002 (2010).
[64] Tang, J. and Wang, K. W., "Active-passive hybrid piezoelectric networks for vibration control: comparisons and improvement," Smart Mater. Struct. 10(4), 794–806 (2001).
[65] Bergamini, A. E., Zündel, M., Flores Parra, E. A., Delpero, T., Ruzzene, M. and Ermanni, P., "Hybrid dispersive media with controllable wave propagation: A new take on smart materials," J. Appl. Phys. 118(15), 154310 (2015).
[66] Sugino, C., Ruzzene, M. and Erturk, A., "An analytical framework for locally resonant piezoelectric metamaterial plates," Int. J. Solids Struct. 182, 281–294 (2020).
[67] Darabi, A., Collet, M. and Leamy, M. J., "Experimental realization of a reconfigurable electroacoustic topological insulator," arXiv Prepr. arXiv1911.09608 (2019).
[68] Riva, E., Quadrelli, D. E., Cazzulani, G. and Braghin, F., "Tunable in-plane topologically protected edge waves in continuum Kagome lattices," J. Appl. Phys. 124(16), 164903 (2018).
[69] Zhou, W., Wu, B., Chen, Z., Chen, W., Lim, C. W. and Reddy, J. N., "Actively controllable topological phase transition in homogeneous piezoelectric rod system," J. Mech. Phys. Solids 137, 103824 (2020).
[70] Meirovitch, L., [Anlaytical Methods in Vibrations], MacMillan, New York, New York (1967).
[71] Graff, K., [Wave Motion in Elastic Solids], Dover Publications (1991).
[72] Tiersten, H. F., [Linear Piezoelectric Plate Vibrations: Elements of the Linear Theory of Piezoelectricity and the Vibrations Piezoelectric Plates], Springer (2013).
[73] Xiao, Y., Wen, J. and Wen, X., "Flexural wave band gaps in locally resonant thin plates with periodically attached spring-mass resonators," J. Phys. D. Appl. Phys. 45(19), 195401 (2012).
[74] Yao, W., Yang, S. A. and Niu, Q., "Edge states in graphene: From gapped flat-band to gapless chiral modes," Phys. Rev. Lett. 102(9), 096801 (2009).
[75] Zhou, S. Y., Gweon, G.-H., Fedorov, A. V., First, P. N., De Heer, W. A., Lee, D.-H., Guinea, F., Castro Neto, A. H. and Lanzara, A., "Substrate-induced bandgap opening in epitaxial graphene," Nat. Mater. 6(10), 770–775 (2007).
[76] Berry, M. V., "Quantal phase factors accompanying adiabatic changes," Proc. R. Soc. London. A. Math. Phys. Sci. 392(1802), 45–57 (1984).